Journal of Marine Research, 48, 437–469, 1990

Journal of
MARINE RESEARCH

Volume 48, Number 3

The thermocline as an "internal boundary layer"

by Rick Salmon[1]

ABSTRACT

In this paper, we analyze one-, two- and three-dimensional numerical solutions of a simple, inertia-less ocean circulation model. The solutions, which all approach a steady state, demonstrate that, in the limit of vanishing thermal diffusivity κ, a front of thickness $\kappa^{1/2}$, identifiable with the thermocline, spontaneously appears at a location anticipated by simple arguments that treat the front as an "internal boundary layer." The temperature and velocity are generally discontinuous across the front, but the velocity component normal to the front is zero. In the asymptotic limit of vanishing diffusivity, the temperature has no vertical variation within the layer above the front, and the potential vorticity is correspondingly zero. The appearance of a front seems to require that the horizontal advection terms cancel in the temperature equation, i.e., that the horizontal velocity be directed along the isotherms on level surfaces. When the surface boundary conditions are specially chosen to prevent this cancellation, the front does not appear. However, in the more realistic cases in which the flow determines its own surface temperature, the cancellation occurs spontaneously and appears to be generically associated with the front.

1. Introduction

Theorists have shown a great fondness for ocean circulation models that consist of two or more immiscible layers with different, constant mass densities. The layers are separated by surfaces (which we will call *fronts*) at which the density jumps between its values in the layers. When only two such layers are present, the single front is usually considered to be a model of the ocean's main thermocline, the region of relatively rapid temperature change between warm surface waters and the cold abyss. Since the observed thermocline is typically several hundred meters thick, this abstrac-

1. Scripps Institution of Oceanography, A-025, La Jolla, California 92093, U.S.A.

tion is severe. When more than two model layers are present, then the layers comprise a crude model of the continuous density field that is actually observed.

In this paper we examine one-, two- and three-dimensional numerical solutions of an inertia-less ocean circulation model in which all the variables, including the mass density, are assumed to be continuous functions of location. The solutions, which all approach a steady state, demonstrate that, in the limit of vanishing thermal diffusivity κ, a front of thickness $\kappa^{1/2}$, identifiable with the thermocline, spontaneously appears at a location anticipated by simple arguments that treat the front as an "internal boundary layer." The temperature and velocity are generally discontinuous across the front, but the velocity component normal to the front must be zero. In the asymptotic limit, the temperature has no vertical variation within the layer above the front (i.e. the potential vorticity is uniformly zero), but horizontal temperature variations are allowed. The existence of a front thus seems to require that the horizontal advection terms cancel in the temperature equation, i.e., that the horizontal velocity be directed along the isotherms on level surfaces. In fact, when the surface boundary conditions are specially chosen to prevent this cancellation, a front does not appear. However, in the more realistic cases in which the flow determines its own surface temperature, this cancellation occurs spontaneously and appears to be generically associated with the front.

The existence of the front clearly depends upon the nonlinear advection terms in the equation for ocean temperature: These are the only nonlinearities present in the inertia-less models considered, and "internal boundary layers" cannot occur in a completely linear model. However, the location of the front is determined by boundary conditions. The front is therefore closely analogous to the movable singularities that appear in the solutions of some nonlinear ordinary differential equations. On the other hand, the frictional *boundary* layers, which are also present in linearized models but always occur at the same locations, are analogous to the fixed singularities that appear at the locations of the singularities in the coefficients of linear ordinary differential equations.

This paper is organized as follows. Section 2 introduces the basic model equations (2.5), and discusses their relationship to the more standard primitive equations (2.1) and to the more restrictive *thermocline equations* (2.14). In Section 3 we analyze a family of very simple, one-dimensional solutions to the thermocline equations in which the horizontal advection of temperature is assumed to be zero. These solutions, which turn out to be the prototype for the more complicated two- and three-dimensional solutions of later sections, exhibit a sharp front at a constant depth. The results of Section 3 are complementary to those of Stommel and Webster (1962) and Young and Ierley (1986).

Section 4 generalizes the one-dimensional model of Section 3 to a two-dimensional model in the vertical and eastward directions, in which the temperature and velocity are independent of latitude, and the eastward velocity is zero. In the solutions of Section 4, the front has a generally nonzero slope in the eastward direction, and, in the

limit of a piecewise-constant temperature at the surface, it closely resembles the sloping interface between homogeneous layers in the familiar two-layer model.

In Section 5 we investigate a second two-dimensional model in which the variables have a prescribed dependence on eastward distance. Friction is still omitted, but the horizontal advection of temperature can now be significant. Since the eastward dependence of the flow is prescribed, the northward dependence of the surface boundary conditions controls the cancellation between the horizontal temperature advection terms. We find that, when the boundary conditions favor cancellation, the solution is essentially the same as in Section 3, and a sharp front occurs. More interestingly, when the boundary conditions do not favor cancellation, the front disappears. The experiments of Section 5 thus establish a connection between the existence of the front and the alignment of the horizontal velocity with isotherms. However, only three-dimensional experiments, in which the fluid determines its own structure in both horizontal directions, can decide whether fronts occur spontaneously.

Solutions of the full three-dimensional equations, including viscosity, are examined in Section 6. These experiments show that the formation of fronts and the coincidence between horizontal streamlines and isotherms are indeed generic, and always occur in regions of Ekman downwelling. Section 7 summarizes the results and their implications for modeling.

This paper makes no pretense to a complete understanding of the solutions to the full inertia-less equations (2.5). Instead we focus on the general character of the front away from coastlines and outcrops, and on the ways in which this front may constrain the flow. The simple "theory" advanced below seems to explain the numerical results, but it certainly lacks a fundamental justification. In fact, I have no explanation for what is surely the most dramatic property of these inertia-less equations, namely, that in all the numerical experiments I have performed, the solutions converge to a steady state, despite high-order nonlinearity.

The numerical experiments reported here are a thin cross section of many experiments performed since 1984. Besides their simplified dynamics and frictional boundary layer structure, these experiments are distinguished from others in the literature by their high spatial resolution in the vertical direction.

2. The simplified model

The primitive equations of ocean motion, invoking the beta-plane, traditional, and Boussinesq approximations, are:

$$\begin{aligned} \frac{D\mathbf{u}}{Dt} + \mathbf{f} \times \mathbf{u} &= -\nabla\phi + A_h\nabla^2\mathbf{u} + A_v\mathbf{u}_{zz} \\ 0 &= -\phi_z + \theta + A_h\nabla^2 w + A_v w_{zz} \\ u_x + v_y + w_z &= 0 \\ \theta_t + u\theta_x + v\theta_y + w\theta_z &= K_h\nabla^2\theta + K_v\theta_{zz}. \end{aligned} \tag{2.1}$$

As usual, (x, y, z) are Cartesian coordinates in the (east, north, up) direction, t is time, $\mathbf{u} = (u, v)$ is the horizontal velocity, w the vertical velocity, $\mathbf{f}$ is the coriolis parameter (times the vertical unit vector), ϕ is the pressure divided by the mean density, θ is the buoyancy (which we will call temperature), and $\nabla = (\partial_x, \partial_y)$. Coordinate subscripts denote differentiation. The parameters A_h, A_v and K_h, K_v are eddy coefficients of viscosity and temperature diffusion in the horizontal and vertical directions. Despite greatly simplified thermodynamics, the equations (2.1), with appropriate boundary conditions, are a relatively complete set of model equations for the large-scale ocean circulation.

In this paper we consider a rectangular ocean governed by the simplified equations:

$$\begin{aligned} \mathbf{f} \times \mathbf{u} &= -\nabla\phi - \Lambda\mathbf{u} + \mathbf{f} \times \mathbf{u}_E \\ 0 &= -\phi_z + \theta - \Lambda w \\ u_x + v_y + w_z &= 0 \\ \theta_t + u\theta_x + v\theta_y + w\theta_z &= K_h\nabla^2\theta + K_v\theta_{zz} \end{aligned} \tag{2.2}$$

which differ from (2.1) in that the horizontal acceleration terms have been entirely omitted, and the eddy viscosity terms have been replaced by Rayleigh friction in all three directions. As explained further below, the $\mathbf{u}_E$-term in (2.2a) represents the momentum put in by wind acting near the surface. Salmon (1986), hereinafter S86, analyzed solutions of equations very similar to (2.2) which had been *linearized* about a state of rest and horizontally uniform temperature. In the present paper, which can be considered a sequel to S86, the emphasis is on the new phenomena that occur when the full nonlinear advection of temperature is retained in (2.2d).

A good way to understand the relationship of (2.2) to (2.1) is to examine the limit of vanishing friction in each. When A_h, $A_v \neq 0$, solutions of (2.1) satisfy velocity boundary conditions of no-normal-flow and no-slip (or prescribed stress). When A_h, $A_v = 0$, (2.1) can still satisfy boundary conditions of no-normal-flow. In contrast, solutions of (2.2) satisfy only the boundary condition of no-normal-flow and require $\Lambda \neq 0$ to do so. With boundary conditions of no-normal-flow, the inviscid limit of (2.2) is singular in the sense that the horizontal velocity tangent to boundaries becomes infinite. From a heuristic viewpoint, this singular behavior arises because the neglect of *both* inertia and friction from (2.1a) leaves a dynamics in which fluid particles respond to force by moving at right angles to the force at a speed proportional to the force. A rigid wall presents a potentially infinite force to the fluid particles that attempt to cross it, and hence the infinite tangential velocity. However, it is unnecessary to keep the full Fickian viscosity of (2.1) to avoid this singular behavior. If *only* the boundary condition of no-normal-flow is required, i.e., if fluid particles can be allowed to slip along the boundary at finite speed, then the simpler Rayleigh friction of (2.2) suffices.

Of course, both the Fickian and Rayleigh eddy viscosities lack any fundamental

justification as parameterizations of the exact Reynolds momentum flux divergence. However, the Rayleigh friction offers the practical advantage that (2.2) has a much simpler boundary layer structure than (2.1). This simplifies the analysis of the boundary layers (as in the linearized solutions examined in S86), but, even more significantly, it greatly facilitates numerical solutions of the inertia-less dynamics. In numerical solutions, all boundary layers must be resolved, or the solutions show spurious behavior that typically includes a change in the sign of the velocity at alternating gridpoints. The need to resolve all three of the nested coastal boundary layers that generally occur in solutions of (2.1) may require the eddy coefficients to be so large that the solutions are unrealistically diffusive. In this paper, we are specifically interested in the nature of the solutions to (2.2) for small values of the friction and diffusivity.

Since (2.2) do not accommodate boundary conditions of prescribed stress, the right-hand side of (2.2a) must include a "body force" component

$$\mathbf{f} \times \mathbf{u}_E(x, y, z) \tag{2.3}$$

which models the input of wind momentum near the surface. As shown in S86, $\mathbf{u}_E(x, y, z)$ can be interpreted as the horizontal correction velocity in a surface Ekman layer of prescribed thickness. Since the Ekman layer is independent of Λ, it is not, strictly speaking, a boundary layer of (2.2).

We nondimensionalize (2.2) in a standard way by scaling

$$\begin{aligned} (x, y) &= L(x', y'), \qquad z = Hz', \qquad t = \frac{L}{U} t' \\ (\mathbf{u}, \mathbf{u}_E) &= U_0(\mathbf{u}', \mathbf{u}_E'), \qquad w = W_0 w', \qquad W_0 = \frac{H}{L} U_0 \\ \phi &= f_0 U_0 L \phi', \qquad \theta = \Delta\theta \cdot \theta'. \end{aligned} \tag{2.4}$$

Here, L and H are, respectively, the ocean width and depth, and $(U_0, W_0, f_0, \Delta\theta)$ are representative values of the (horizontal velocity, vertical velocity, coriolis parameter, basin-scale temperature variation). Then, after dropping primes, (2.2) take the form,

$$\begin{aligned} \mathbf{f} \times \mathbf{u} &= -\nabla\phi - \epsilon\mathbf{u} + \mathbf{f} \times \mathbf{u}_E \\ 0 &= -\phi_z + T\theta - \epsilon\delta^2 w \\ u_x + v_y + w_z &= 0 \\ \theta_t + u\theta_x + v\theta_y + w\theta_z &= \kappa_h(\theta_{xx} + \theta_{yy}) + \kappa_v\theta_{zz} \end{aligned} \tag{2.5}$$

where

$$\epsilon = \frac{\Lambda}{f_0}, \qquad \delta = \frac{H}{L}, \qquad \kappa_h = \frac{K_h}{U_0 L}, \qquad \kappa_v = \frac{K_v}{W_0 H} \tag{2.6}$$

and

$$f = 1 + \beta\left(y - \frac{1}{2}\right), \qquad \beta = \frac{\beta_{\text{dim}} L}{f_0} \tag{2.7}$$

where β_{dim} is the dimensional value of df/dy. The complete boundary conditions on (2.5) are no-normal-velocity and prescribed temperature or heat flux at all boundaries. Colin de Verdiere (1988, 1989) has analyzed interesting numerical solutions of equations that are very similar to (2.5) but include Fickian diffusion of horizontal momentum. He calls these equations the *planetary geostrophic equations*.

In interesting cases, the parameters (2.6) are all small compared to unity, and β is order one. The nondimensional parameter

$$T = \frac{\delta^2 \Delta\theta}{W_0 f_0} \tag{2.8}$$

is a measure of the ratio of thermohaline to wind forcing, with the scales $\Delta\theta$ and W_0 set by the differential heating and Ekman pumping near the ocean surface. By an argument of Welander (1971), T controls the depth of the thermocline. Briefly, the (dimensional) Sverdrup relation,

$$\beta v = f \frac{\partial w}{\partial z} \tag{2.9}$$

implies that

$$\beta U_0 \sim \frac{f_0 W_0}{h} \tag{2.10}$$

where h is the depth of the thermocline. By the thermal wind relationship,

$$f \frac{\partial v}{\partial z} = \frac{\partial \theta}{\partial x} \tag{2.11}$$

we have

$$\frac{f_0 U_0}{h} \sim \frac{\Delta\theta}{L}. \tag{2.12}$$

Eliminating U_0 between (2.10) and (2.12) yields

$$\frac{h}{H} \sim \sqrt{\frac{f_0^2 W_0 L}{\beta_{\text{dim}} \Delta\theta H^2}} = \frac{1}{\sqrt{\beta T}}. \tag{2.13}$$

We shall recover (2.13) in numerous special cases. From here onward we adopt the somewhat more natural convention of formally setting $T = 1$ in (2.5), and forcing θ to

be order T by the boundary conditions. The nondimensional thermocline depth in the subtropical ocean is about $1/7$. Thus by (2.13) T is of order 50. However, to center the thermocline within the computational domain of our numerical experiments, we shall usually force T to be of order 10 (but still large compared to unity).

In my opinion, no set of equations simpler than (2.5) can consistently model the circulation of an entire ocean basin. Numerical solutions of the full Eqs. (2.5), with thermal forcing and penetrative convection appended, will be presented in a later article. In this paper, we consider various abridgments to (2.5) that may apply to restricted regions. Our basic abridgment is to consider the flow below the Ekman layer only, and thus to exclude the horizontal Ekman transport. This abridgment corresponds to setting $\mathbf{u}_E = 0$ in (2.5a) and replacing the upper boundary condition $w = 0$ by a prescribed Ekman upwelling or downwelling.

A further abridgment will consist of omitting the friction terms from (2.5a–b) altogether. There results the *thermocline equations*,

$$\begin{aligned} \mathbf{f} \times \mathbf{u} &= -\nabla\phi \\ 0 &= -\phi_z + \theta \\ u_x + v_y + w_z &= 0 \\ \theta_t + u\theta_x + v\theta_y + w\theta_z &= \kappa_h(\theta_{xx} + \theta_{yy}) + \kappa_v\theta_{zz}. \end{aligned} \tag{2.14}$$

The boundary conditions on (2.14) are the matching conditions to boundary layers or fronts in which the viscosity is important.

The *ideal thermocline equations*, obtained by setting $\kappa_h, \kappa_v = 0$ in (2.14), represent an even more drastic abridgment of (2.5). The ideal thermocline equations apply only to the regions between all boundary layers and fronts. An important conclusion of this paper will be that ideal thermocline equations do not apply over the whole interior of the ocean.

In the most general case, we solve (2.5) on $0 < x, y, z < 1$ by stepping (2.5d) forward in time, and then determining the velocity field at the new time from the solution of a linear elliptic equation obtained from (2.5a–c). If $\epsilon \ll 1$, then (2.5a–b) imply that

$$\begin{aligned} u &\approx -\frac{1}{f}\phi_y - \frac{\epsilon}{f^2}\phi_x + u_E \\ v &\approx +\frac{1}{f}\phi_x - \frac{\epsilon}{f^2}\phi_y + v_E \\ w &= \frac{\theta - \phi_z}{\epsilon\delta^2} \end{aligned} \tag{2.15}$$

so that the mass conservation equation (2.5c) becomes

$$\epsilon\delta^2\left[\frac{\beta}{f^2}\phi_x + \nabla\cdot\left(\frac{\epsilon}{f^2}\nabla\phi\right) - \nabla\cdot\mathbf{u}_E\right] + \phi_{zz} = \theta_z \tag{2.16}$$

with boundary conditions of no-normal flow,

$$\frac{\partial \phi}{\partial s} + \frac{\epsilon}{f}\frac{\partial \phi}{\partial n} = f\mathbf{u}_E \cdot \mathbf{n} \qquad \text{at coasts}$$
$$\frac{\partial \phi}{\partial z} = \theta \qquad \text{at } z = 0, 1. \tag{2.17}$$

Here, $\mathbf{n}$ is the outward unit normal at the coast, and s is distance measured counterclockwise along the coast. As in S86, we solve (2.16–17) for ϕ by expanding ϕ and θ_z in vertical cosine series, and then solving the two-dimensional elliptic equation for each vertical mode by sequential over-relaxation. After each pass through the interior gridpoints, all the boundary points are updated *simultaneously* by use of (2.17a); this requires the easy solution of a "wrapped-around" tridiagonal system.

We are interested in the case of asymptotically small friction ϵ and diffusion κ. Since ϵ multiplies only horizontal derivatives in (2.16), we anticipate that the friction is negligible outside sidewall boundary layers and (possibly) some fronts. The boundary layer structure of linearized equations similar to (2.5) was explored in S86, and some of that analysis applies to (2.5). For the flat-bottom case considered, the depth-averaged flow is unaffected by θ and is hence the same for both the linear and nonlinear cases. The boundary layers on the depth-averaged flow include a western boundary layer of thickness ϵ and northern and southern boundary layers of thickness $\epsilon^{1/2}$. There is no eastern boundary layer on the depth-averaged flow, and the interior depth-averaged velocity must therefore obey the boundary condition $u = 0$ at $x = 1$.

To analyze the boundary layer structure of the non-depth-averaged flow, we first note that if θ is *smooth,* i.e., if the temperature includes no spatial scales as small as the boundary layer scale, then all frictional boundary layers can be analyzed on the basis of (2.16) alone. The hypothesis of smooth θ is clearly dangerous in view of the coupling between the velocity and temperature introduced by (2.5d), and in fact does not apply to linear theory. However, numerical solutions of the nonlinear model (2.5) suggest that regions of rapid temperature variation do not often coincide with regions in which friction is important. Separated western boundary currents are a notable exception.

For smooth θ, the coastal boundary layers on the non-depth-averaged flow have the same correction equations as in the case of homogeneous flow (S86, Section 4), and exist at *any* coast where either the Ekman transport or the interior thermal wind has a component normal to the coastline. These boundary layers, which we call *upwelling layers,* have a thickness $\epsilon\delta$, vertical velocities of order $1/(\epsilon\delta)$, and longshore geostrophic currents of order $1/\epsilon$. The important point here is that, since the upwelling layers can accept an order-one normal flow from the interior, the interior non-depth-averaged flow need not have a zero normal component at any coastline, including the eastern boundary at $x = 1$. This means that the only coastal boundary condition on velocity in the thermocline equations (2.14) is that the *depth-averaged* eastward velocity be zero at $x = 1$. Pedlosky (1983), Janowitz (1986), and Huang (1989) have previously

emphasized the importance of allowing a nonzero interior baroclinic flow at the eastern boundary.

The great utility of the thermocline equations stems from the fact that (2.14) can be rewritten as a single scalar equation in a single unknown (Welander, 1971). First, the Sverdrup relation (2.9) is rewritten in the divergence form

$$\frac{\partial}{\partial x}(\phi) = \frac{\partial}{\partial z}\left(\frac{f^2}{\beta} w\right). \tag{2.18}$$

This motivates the definition

$$\phi = \frac{\partial M}{\partial z}, \qquad w = \frac{\beta}{f^2}\frac{\partial M}{\partial x}. \tag{2.19}$$

By (2.14a–b)

$$u = -\frac{1}{f} M_{yz}, \qquad v = \frac{1}{f} M_{xz}, \qquad \theta = M_{zz} \tag{2.20}$$

and thus (2.14d) becomes

$$fM_{zzt} - M_{yz}M_{zzx} + M_{xz}M_{zzy} + \frac{\beta}{f} M_x M_{zzz} = f[\kappa_h \nabla^2 M_{zz} + \kappa_v M_{zzzz}]. \tag{2.21}$$

The factors f and β/f can, if desired, be absorbed into the definitions of y and κ in (2.21) to obtain an equation

$$fM_{zzt} - M_{yz}M_{zzx} + M_{xz}M_{zzy} + M_x M_{zzz} = \mu_h \nabla^2 M_{zz} + \mu_v M_{zzzz} \tag{2.22}$$

in which f, μ_h, μ_v are the only nonconstant coefficients. Then, since our solutions all approach a steady state, it makes no difference if we replace f by unity in the first term of (2.22).

3. A one-dimensional prototype

Our first example is probably the simplest special case that exhibits a front. Consider the flow below the Ekman layer and away from the sidewalls, and assume that the governing equations are the thermocline equations (2.14) or (2.21). We consider the special solution

$$M = xW(z) \tag{3.1}$$

for which

$$\phi = xW', \qquad u = 0, \qquad v = \frac{1}{f} W', \qquad w = \frac{\beta}{f^2} W, \qquad \theta = xW'' \tag{3.2}$$

and (2.21) becomes

$$WW_{zzz} = \mu W_{zzzz} \tag{3.3}$$

where

$$\mu = \frac{f^2 \kappa_v}{\beta} \tag{3.4}$$

is a small parameter with parametric y-dependence. Eq. (3.3), which seems to be the prototype for the more complicated cases studied below, expresses a balance between vertical advection $w\theta_z$ and vertical diffusion $\kappa_v \theta_{zz}$ of temperature. The horizontal advection terms are absent because the eastward velocity and northward temperature gradient are zero.

We imagine (3.3) to hold between the bottom of the Ekman layer and either the bottom of the ocean or the top of an abyssal layer with different dynamics. The boundary conditions are prescribed vertical velocity and temperature at these two boundaries:

$$\begin{aligned} W(1) &= w_E, \qquad W''(1) = T_E \\ W(0) &= w_B, \qquad W''(0) = T_B. \end{aligned} \tag{3.5}$$

We must prescribe the temperatures at both boundaries because horizontal advection (which could maintain a temperature contrast) has been neglected. If the temperature boundary condition at one of the boundaries were changed to no-flux, then the temperature would always become uniform at the temperature of the other boundary.

The surface and bottom temperatures are xT_E and xT_B respectively. For static stability, we want $T_E > T_B$ if the ocean lies on $x > 0$, and $T_E < T_B$ if the ocean lies on $x < 0$. (It is more convenient to let the east–west location of the model ocean be arbitrary than to replace x by $x - x_0$ in (3.1).) If the horizontal temperature variation at the bottom is to be less than at the top (a reasonable assumption) then we also want the absolute value of T_B to be less than the absolute value of T_E. We shall often assume that $T_B = 0$. Then if the ocean lies on $-1 < x < 0$, we require that $T_E < 0$. This corresponds to an ocean with a constant temperature on the bottom and eastern sidewall, and a surface temperature that is warmest on the western side of the ocean. If the ocean lies on $0 < x < 1$, we require $T_E > 0$, corresponding to an ocean with a constant temperature on the bottom and western sidewall, and a surface temperature that is warmest on the eastern side of the ocean.

The equation (3.3) has been solved by stepping the time-dependent form

$$W_{zzt} + WW_{zzz} = \mu W_{zzzz} \tag{3.6}$$

to equilibrium. This system always approaches a steady state. The time-dependent equation (3.6) bears a resemblance to Burger's equation (which would be obtained by erasing two z-derivatives from every term in (3.6)), but whereas the solutions to

Burger's equation contain only *moving* fronts, (3.6) exhibits stationary fronts in its equilibrium solutions.

At equilibrium, and outside boundary layers or fronts, W obeys the "outer" equation

$$WW_{zzz} = 0. \tag{3.7}$$

Thus, in outer regions,

$$W_{zzz} = 0 \tag{3.8}$$

and

$$W = Az^2 + Bz + C. \tag{3.9}$$

The constants A, B, and C are generally different in each outer region. However, since three constants cannot generally satisfy the four boundary conditions (3.5), there must exist at least one boundary layer or front.

The analysis of the boundary layers and fronts is complicated by the fact that the inner equation is the full equation (3.3). We make some progress by assuming that it is permissible to replace the *undifferentiated* W in (3.3) by a truncated Taylor expansion. This method, which is ad hoc, was suggested by the fact that the boundary layers and fronts are visible only in the higher derivatives of W in the numerical solutions of (3.6), while W itself appears to be everywhere smooth. Let the location of the inner region be z_0. If $z_0 \neq 0, 1$ then the inner region is a front rather than a boundary layer. With the hypothesis introduced above, the inner equation is a linear equation,

$$(W_0 + W_1(z - z_0) + \cdots)W_{zzz} = \mu W_{zzzz} \tag{3.10}$$

where

$$W_n = W^{(n)}(z_0) \tag{3.11}$$

is the n-th derivative of W. Then

$$W_{zzz} = \text{const} \exp\left[W_0 \frac{(z - z_0)}{\mu} + W_1 \frac{(z - z_0)^2}{2\mu} + \cdots\right] \tag{3.12}$$

and three further integrations would complete the solution. If $W_0 \neq 0$, then the W_1 term is negligible, and the thickness of the inner region is μ. However, in this case, we must have $z_0 = 0$ or 1, because the inner region correction decays only in one direction. In fact, if W_0 is positive, we must have $z_0 = 1$, and if W_0 is negative, we must have $z_0 = 0$.

If $W_0 = 0$, then

$$W_{zzz} = \text{const} \exp\left[W_1 \frac{(z - z_0)^2}{2\mu}\right] \tag{3.13}$$

and the inner-layer correction decays in both directions provided that $W_1 < 0$. The inner region then has thickness $\mu^{1/2}$, and all higher terms in (3.12) are negligible. This type of inner region can occur at any z_0 where W_0 is zero and W_1 is negative.

Anticipating that the outer solution must satisfy the boundary conditions on W (but not on W_{zz}), we can summarize our predictions as follows. Boundary layers of thickness μ can occur at any boundary at which fluid is *leaving* the domain. Fronts or boundary layers of thickness $\mu^{1/2}$ can occur at any depth where $W = 0$ and W_z is negative.

Using these rules on the locations of the inner regions, we can construct a theory of the outer solutions. Suppose that $w_B = T_B = 0$. Then it is obvious from (3.3, 3.5) that, in outer regions, W/w_E depends only upon the ratio w_E/T_E. A top boundary layer appears possible when $w_E > 0$ (Fig. 1a). In that case, the outer solution

$$W = w_E z, \quad \text{all } z \tag{3.14}$$

satisfies all boundary conditions except the surface boundary condition on temperature.

On the other hand, if a bottom boundary layer exists, then the outer solution must be

$$W = \tfrac{1}{2} T_E(z-1)^2 + (w_E + \tfrac{1}{2} T_E)(z-1) + w_E, \qquad \text{all } z \tag{3.15}$$

which satisfies all boundary conditions except the bottom boundary condition on the temperature. However, since $w_B = 0$, a bottom boundary layer can exist only when $dW/dz < 0$ at $z = 0$, i.e., when

$$T_E > 2w_E. \tag{3.16}$$

Refer again to Figure 1a. This leaves the nature of the solution undetermined in two sectors of the w_E–T_E plane. In a sector of the first quadrant, both (3.14) and (3.15) seem possible. In a sector of the third quadrant, neither (3.14) nor (3.15) is possible.

In the third quadrant sector, the inner region must be a front. Let z_0 be the location of the front. The outer solutions are

$$\begin{aligned} W &= W^+ \equiv \tfrac{1}{2} T_E(z-1)^2 + A(z-1) + w_E, \qquad z > z_0 \\ W &= W^- \equiv Bz, \qquad z < z_0 \end{aligned} \tag{3.17}$$

where the constants A and B must be determined. It is easily shown that the outer solutions and their first derivatives must match at z_0. Thus, using the fact that $W_0 = 0$ at the front, we have

$$W^+ = W^- = 0 \qquad \text{and} \qquad W_z^+ = W_z^- \qquad \text{at } z_0. \tag{3.18}$$

These three conditions determine the three constants A, B, and z_0. We find that

$$\begin{aligned} W &= W^+ \equiv \tfrac{1}{2} T_E(z-1)^2 - T_E(z_0 - 1)(z-1) + w_E, \qquad z > z_0 \\ W &= W^- \equiv 0, \qquad z < z_0 \end{aligned} \tag{3.19}$$

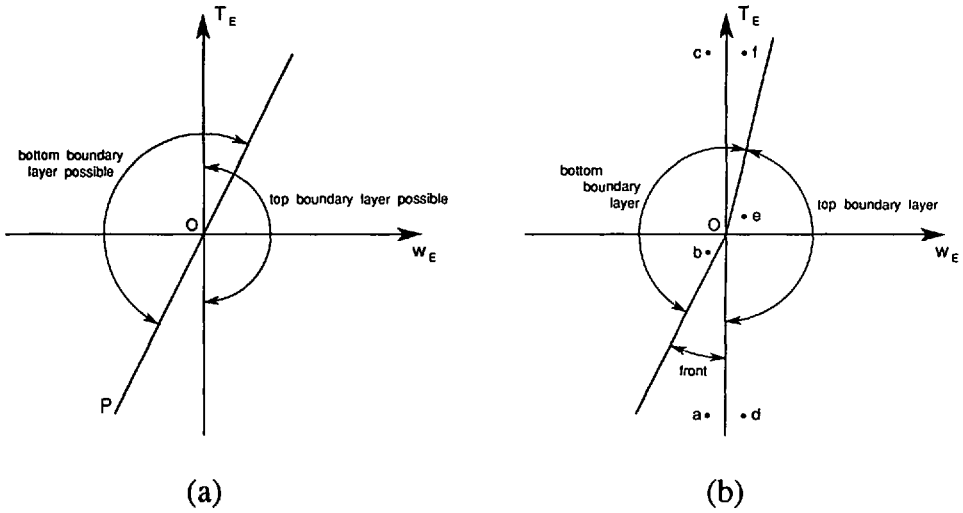

Figure 1. (a) The regions of the w_E-T_E plane in which solutions of the one-dimensional thermocline equation (3.3, 3.5) with top and bottom boundary layers are apparently possible, and (b) the types of solutions that actually occur. w_E is the vertical velocity at the base of the Ekman layer, and T_E is the eastward derivative of the surface temperature.

where the depth h of the front is given by

$$h \equiv 1 - z_0 = \sqrt{\frac{2w_E}{T_E}}. \tag{3.20}$$

The solution (3.19) matches smoothly to (3.15) along the line OP in Figure 1a, and also to (3.14) along the negative T_E-axis.

In contrast, (3.14) and (3.15) do not match smoothly along any bounding radius within the first quadrant region of overlap. Numerical experiments show that the location of the boundary layer changes rapidly (but continuously) from the bottom to the top along the line $T_E \approx 4.2w_E$. Near this line, numerical solutions of (3.6) equilibrate very slowly. A complete map of the solutions is given in Figure 1b.

Figure 2 shows representative solutions from each region of Figure 1b for the case $\mu = .01$. This value of μ corresponds to realistic scale sizes of $K_v = 1$ cm^2 sec^{-1}, $H =$ 5 km, and $W_0 = 2 \times 10^{-4}$ cm sec^{-1}. Outside the inner regions, the solutions in Figure 2 agree closely with the outer solutions predicted above. Other solutions (not presented here) show that these results are little changed if w_B, T_B take small nonzero values.

The most interesting cases are those that exhibit a front. They correspond to Ekman downwelling at the surface ($w_E < 0$) and a surface temperature that increases to the west at a sufficiently rapid rate ($T_E < 2w_E$). Figure 3 shows the solutions corresponding to $w_E = -1$ and $T_E = -10$ for three values of μ. Because the front has a relatively large ($\mu^{1/2}$) thickness, it is not easily recognized as an "internal boundary layer" in the solution with the largest (most realistic) value of μ (Fig. 3, curve *a*). In fact, judging by

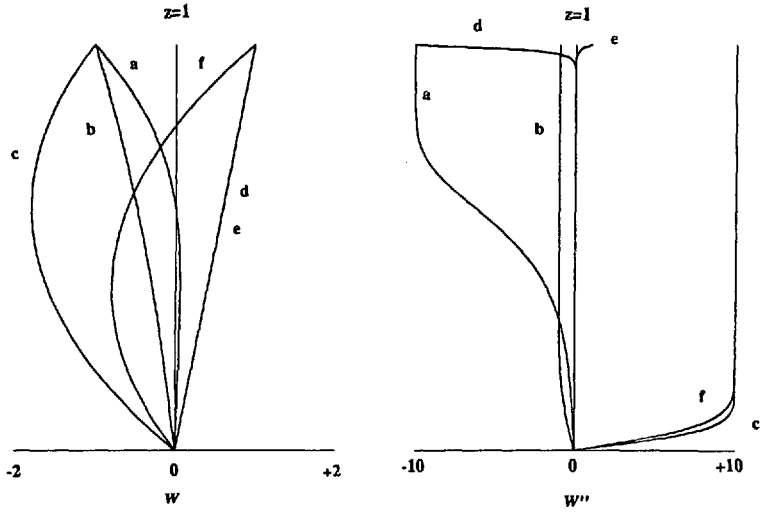

Figure 2. The vertical velocity $W(z)$ satisfying (3.3), and its second derivative W''. The boundary conditions are (3.5) with $w_B = T_B = 0$ and (a) $w_E = -1$, $T_E = -10$; (b) $w_E = -1$, $T_E = -1$; (c) $w_E = -1$, $T_E = 10$; (d) $w_E = 1$, $T_E = -10$; (e) $w_E = 1$, $T_E = 1$; and (f) $w_E = 1$, $T_E = 10$, corresponding to the points a through f on Figure 1b. These boundary conditions correspond to zero vertical velocity and constant temperature at the ocean bottom, Ekman upwelling ($w_E > 0$) or downwelling ($w_E < 0$) at the surface, and surface temperature increasing to the west ($T_E < 0$) or east ($T_E > 0$). The temperature is proportional to the absolute value of W''.

the smooth appearance of curve *a* alone, one might be tempted to guess that diffusion is nowhere important, and that the interior of the ocean could be explained by the *ideal* thermocline equations. However, the "internal boundary layer" character of the front clearly means that diffusion is *always* important. That is, no matter how thick and well-disguised the front, temperature diffusion is clearly necessary to match together the two outer regions in which it is unimportant.

The relatively large thickness of the front for realistic values of μ also means that the asymptotic limit $\mu \to 0$, in which the front becomes a two-dimensional surface, has a limited *quantitative* applicability to the real ocean. But just as the solutions to any differential equation are best characterized by their behavior near singularities, the asymptotic limit of a sharp front offers the best hope for a better *qualitative* understanding of the ocean circulation.

G. R. Ierley (personal communication) has examined numerical solutions of (3.3, 3.5) by the method of "shooting." He confirms the picture described above, but he believes that the "top boundary layer" behavior is actually caused by a simple pole p associated with the special solution

$$W = \frac{4\mu}{(p - z)} \tag{3.21}$$

of (3.3), and lying just above $z = 1$.

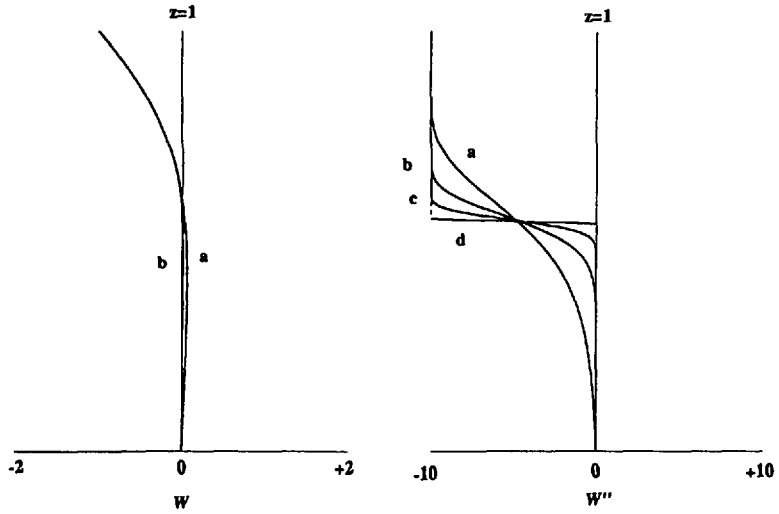

Figure 3. The same as Figure 2, but with $w_B = T_B = 0$, $w_E = -1$, and $T_E = -10$, for three values of the nondimensional diffusivity: (a) $\mu = .01$; (b) $\mu = .001$; (c) $\mu = .0001$; and (d) the outer solution (3.19). As regards W, curves b, c, and d are indistinguishable, and curve a differs slightly from the others below the front.

The existence of a special solution with the form (3.1) has been noted, but not previously studied in detail. Although technically not a similarity solution, it corresponds to the parameter values $k = 0$ and $m = \infty$, respectively, in the families of similarity solutions discovered by Robinson and Stommel (1959) and Young and Ierley (1986). However, our results are very similar to those obtained by Stommel and Webster (1962) and Young and Ierley (1986) for the special form,

$$M = x^{2/3}F(z/x^{1/3}), \qquad \text{i.e.} \qquad \theta = \theta(z/x^{1/3}) \tag{3.22}$$

The differences between (3.1) and (3.22) are that (3.1) yields a simpler equation, (3.3), and applies to an ocean of finite depth in which the eastern and bottom boundary conditions need not be combined. Young and Ierley attributed the front to a conflict between the boundary conditions at the top and those at the eastern boundary. In this paper, the conflict is between the top and bottom boundary conditions. As argued in Section 2, there seems to be no reason to require that the interior, non-depth-averaged eastward velocity be zero at $x = 1$. In both solutions, the horizontal advection of temperature is zero.

In the next two sections we examine two distinct, *two-dimensional* families of solutions to the thermocline equations. These two-dimensional models generalize the one-dimensional prototype (3.1) to the forms

$$M = M(x, z) \tag{3.23}$$

and

$$M = xW(y, z). \tag{3.24}$$

The model (3.23) of Section 4 permits the front to have a nonzero east-west slope, but there is still no horizontal advection of temperature. In the model (3.24) of Section 5, horizontal temperature advection can be important.

4. Two-dimensional model with no horizontal advection

We again assume that the flow is governed by the thermocline equations, and consider special solutions of the form

$$M = M(x, z). \tag{4.1}$$

for which

$$\phi = M_z, \qquad u = 0, \qquad v = \frac{1}{f} M_{xz}, \qquad w = \frac{\beta}{f^2} M_x, \qquad \theta = M_{zz} \tag{4.2}$$

With $\mu = \mu_h = \mu_v$ the thermocline equation (2.22) takes the form

$$M_x M_{zzz} = \mu [M_{zzxx} + M_{zzzz}] \tag{4.3}$$

or

$$W\theta_z = \mu [\theta_{xx} + \theta_{zz}], \qquad W_{zz} = \theta_x, \qquad W \equiv M_x \tag{4.4}$$

We solve (4.3) by time-stepping the time-dependent form

$$M_{zzt} + M_x M_{zzz} = \mu [M_{zzxx} + M_{zzzz}] \tag{4.5}$$

The boundary conditions are taken as

$$\begin{aligned} W(x, 1) &= w_E(x), \qquad \theta(x, 1) = \theta_E(x) \\ W(x, 0) &= 0, \qquad \theta(x, 0) = 0 \end{aligned} \tag{4.6}$$

and

$$\theta_x = 0 \qquad \text{at coasts.} \tag{4.7}$$

Once again, the solutions always converge to a steady state. There are no coastal boundary layers, and hence no need for friction, because the eastward velocity u is everywhere zero.

The new feature of these solutions is that the front can have a non-zero slope in the east–west direction. In outer regions, where temperature diffusion is negligible, we must have

$$W = 0 \qquad \text{or} \qquad \theta_z = 0. \tag{4.8}$$

Thus either

$$\theta = F(z) \qquad \text{and} \qquad W = 0 \tag{4.9}$$

or

$$\theta = A(x) \qquad \text{and} \qquad W = \tfrac{1}{2} A'(x)z^2 + B(x)z + C(x) \tag{4.10}$$

where

$$F(z), A(x), B(x), C(x) \tag{4.11}$$

are functions to be determined from the boundary and matching conditions.

The interesting case is $w_E < 0$. If $\theta_E = 0$, the solution

$$\theta = 0, \qquad W = w_E(x)z \tag{4.12}$$

satisfies all boundary conditions. If $\theta_E > 0$ there must be a bottom boundary layer or front. If there is a front at $z = z_0(x) \neq 0$, then we must have

$$\theta = \theta_E(x), \qquad W = \tfrac{1}{2}\theta_E'(x)(z-1)^2 + C(x)(z-1) + w_E(x), \qquad z > z_0 \tag{4.13}$$

and either

$$\theta = F(z), \qquad W = 0, \qquad z < z_0 \qquad (F(0) = 0) \tag{4.14}$$

or

$$\theta = 0, \qquad W = B(x)z, \qquad z < z_0 \tag{4.15}$$

By (4.4), the outer solutions (4.13–15) must also satisfy the jump conditions

$$W = \Delta W = 0 \qquad \text{and} \qquad \Delta W_z = -[\theta_E - F(z_0)]\frac{dz_0}{dx} \tag{4.16}$$

at z_0, where $\Delta W \equiv W(z_0^+) - W(z_0^-)$. We find that

$$\begin{aligned} \theta &= \theta_E(x) \\ W &= [\tfrac{1}{2}\theta_E'(z-1)^2 + (\theta_E h)'(z-1) - F(z_0)h'(z-1)] \\ &\quad + w_E(x), \qquad z > z_0 \end{aligned} \tag{4.17}$$

and

$$\theta = F(z), \qquad W = 0, \qquad z < z_0 \tag{4.18}$$

where the depth

$$h(x) \equiv 1 - z_0(x) \tag{4.19}$$

of the front is determined by

$$\frac{d}{dx}\left(\frac{1}{2}\theta_E h^2\right) - F(z_0)\frac{d}{dx}\left(\frac{1}{2}h^2\right) = w_E. \tag{4.20}$$

The primes on θ_E and h denote x-differentiation.

Suppose that the deep stratification is zero, $F(z) = 0$. Then the solution to (4.20) is

$$h^2 = \frac{2(x - x_0)w_E}{\theta_E(x)} \tag{4.21}$$

where x_0 is a constant of integration. In the special case

$$\theta_E = T_E(x - x_0), \qquad T_E = \text{const} \tag{4.22}$$

we recover the result of Section 3. By (4.2c) and (4.17) the northward velocity is

$$v = \frac{1}{f}[\theta_E'(z - 1) + (h\theta_E)'], \qquad z > z_0 \tag{4.23}$$

above the front and zero below; the eastward velocity is everywhere zero. Note that v is discontinuous across the front only if the frontal slope h' is nonzero.

Numerical solutions of (4.5) always approach a steady state. Two equilibrium solutions will be shown. These exhibit the two extreme types of frontal behavior allowed by the Sverdrup equation (4.20). In the first solution (Fig. 4), the prescribed surface temperature is piecewise constant,

$$\theta_E(x) = \begin{cases} 20, & 0 < x < .5 \\ 0, & .5 < x < 1 \end{cases} \tag{4.24}$$

corresponding to an upper layer of constant temperature. Eq. (4.20) is satisfied with $\theta_E' = 0$ and $h' \neq 0$. In the second numerical solution (Fig. 5), the surface temperature varies continuously,

$$\theta_E(x) = \begin{cases} 20\left(1 - \dfrac{x}{.75}\right), & 0 < x < .75 \\ 0, & .75 < x < 1 \end{cases} \tag{4.25}$$

and (4.20) is satisfied with $\theta_E' \neq 0$ and $h' = 0$. In both experiments $w_E = -1$, and the bottom temperature and vertical velocity are zero. The resolution is 100×100 gridpoints, and the diffusivity is $\mu = .005$.

The numerical experiments confirm the behavior predicted above. The temperature field in the homogeneous-layer experiment (4.24) is shown in Figure 4a. The computed thermocline depth closely agrees with that predicted by (4.21) with $x_0 = .5$. The vertical velocity (Fig. 4b) is small below the front. East of the frontal outcropping, the

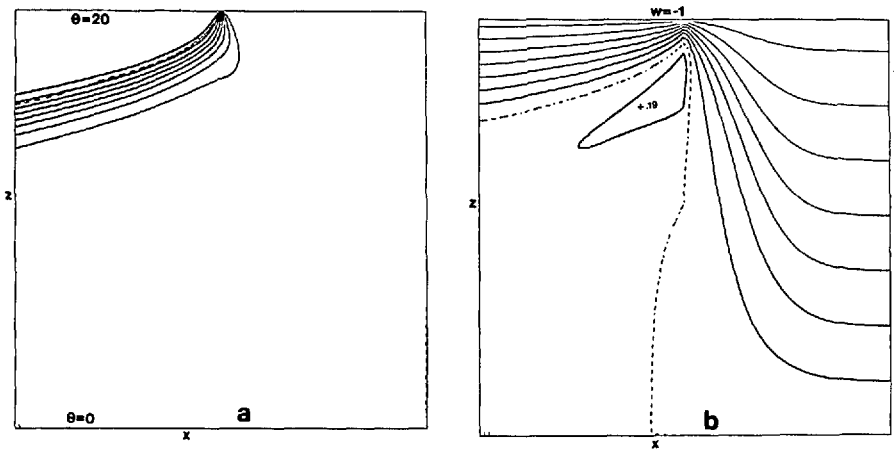

Figure 4. The equilibrium solution of the two-dimensional thermocline model (4.4) and (4.6) for the case of piecewise constant surface temperature (4.24) and surface vertical velocity $w_E = -1$. (a) The computed temperature $\theta(x, z)$ in an east-west section; and (b) the vertical velocity $w(x, z)$. Darker contours denote higher values, and the zero contour is dashed. The dashed line in (a) is the front location predicted by (4.21).

vertical velocity varies linearly with depth, and the solution is the same as for homogeneous fluid.

Figure 4a also shows a narrow region of static instability in the vicinity of the outcrop. Static instability is in fact a typical feature of the equilibrium solutions to the inertia-less equations. In most of the numerical experiments described in this paper, the boundary conditions were arranged to reduce or eliminate static instability. In a later paper, we will consider solutions of (2.5) that include the horizontal Ekman transport $\mathbf{u}_E$ and a surface cooling at high latitude. The latter solutions show large regions of strong static instability unless the dynamics includes an explicit vertical convection. Although the addition of vertical convection complicates the interpretation of the solutions, it does not erase general features like fronts that also occur in the more ideal situations analyzed in this paper.

Figure 5 shows the corresponding equilibrium fields for the case (4.25) of continuous surface temperature. Now (4.21) (with $x_0 = .75$) predicts that the depth of the front has the constant value $h = .27$ shown by the arrow in Figure 5a. Thus the front begins in midwater, at $x = .75$, where the temperature jump across the front is zero. This temperature jump increases linearly to the west. The vertical velocity is small below the front (Fig. 5b), no matter what the size of the temperature jump across the front. East of $x = .75$, the velocity field is again the same as for homogeneous fluid.

Other solutions, not depicted, show that a bottom boundary layer occurs when the prescribed surface temperature increases toward the east. This is anticipated from the results of Section 3.

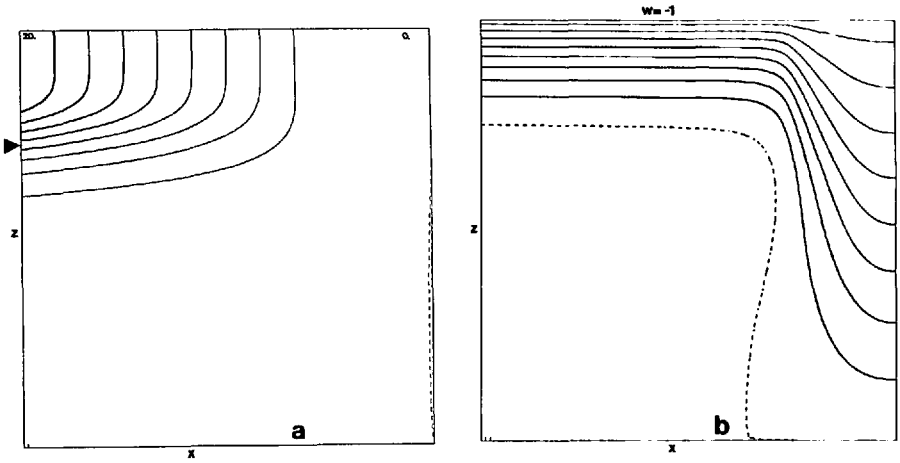

Figure 5. The same as Figure 4, but for the case of continuous surface temperature (4.25). The arrow on (a) is located at the constant depth of the front predicted by (4.21) and (4.25).

The special solutions of this section show that the inertia-less equations exhibit fronts that are considerably more general than the interface between homogeneous layers typically postulated in layered models. However, these special solutions are unrealistic in two major ways. First, the surface temperature has been prescribed, and could not sensibly have been determined by the flow itself. Second, the horizontal advection of temperature was assumed to be zero. The need to prescribe the surface temperature is an unavoidable feature of two-dimensional models, but the neglect of horizontal temperature advection is not. In the next section we examine some two-dimensional solutions in which horizontal temperature advection can be significant.

5. Two-dimensional model with significant horizontal advection

We again assume that the friction is negligible, so that the flow is governed by the thermocline equations in the form (2.22), and consider special solutions of the form

$$M(x, y, z) = xW(y, z) \tag{5.1}$$

for which (2.22) reduces to

$$-W_{zy}W_{zz} + W_zW_{zzy} + WW_{zzz} = \mu[W_{zzyy} + W_{zzzz}]. \tag{5.2}$$

The boundary conditions are taken as

$$\begin{aligned} W(y, 1) &= w_E(y), & W_{zz}(y, 1) &= T_E(y) \\ W(y, 0) &= 0, & W_{zz}(y, 0) &= 0. \end{aligned} \tag{5.3}$$

Eqs. (5.1–3) generalize the one-dimensional problem (3.1–5) considered in Section 3. As in Sections 3 and 4, we solve (5.2–3) by stepping the time-dependent form of (5.2)

to equilibrium. Once again, the solution always approaches a steady state. The new feature of (5.2) is that the horizontal advection of temperature need not be small. Again the interesting case is $w_E < 0$ (Ekman downwelling) and $T_E < 2w_E$ (corresponding to an ocean on $x < 0$ with surface temperature increasing to the west).

Now, if the horizontal advection terms in (5.2) were to cancel, then the solution would be (3.19–20) with w_E, T_E replaced by $w_E(y)$, $T_E(y)$. Then substituting (3.19–20) back into (5.2), we easily find that the horizontal advection terms do indeed cancel only if the surface temperature is proportional to the vertical velocity,

$$w_E(y) = \text{const } T_E(y). \tag{5.4}$$

By (3.20), (5.4) implies that the thermocline has a constant depth. Thus, if the boundary conditions satisfy (5.4), then the horizontal advection is zero, and we obtain our former solution (3.19–20) with the front at a constant depth. If the boundary conditions do *not* satisfy (5.4), then numerical experiments show that the solution does not contain a front.

The two experiments summarized in Figures 6 and 7 are typical. In the experiment of Figure 6, the boundary conditions are

$$\begin{aligned} w_E(y) &= -1 + \tfrac{1}{2}\cos \pi y \qquad (0 < y < 1) \\ T_E(y) &= 10\,(-1 + \tfrac{1}{2}\cos \pi y) \end{aligned} \tag{5.5}$$

which satisfy (5.4). In the experiment of Figure 7, the boundary conditions are

$$\begin{aligned} w_E(y) &= -1 + \tfrac{1}{2}\cos \pi y \\ T_E(y) &= 10(-1 - \tfrac{1}{2}\cos \pi y) \end{aligned} \tag{5.6}$$

which do not satisfy (5.4). In both experiments $\mu = .002$ and the sidewall boundary conditions are

$$W_{zzy}(0, z) = W_{zzy}(1, z) = 0 \tag{5.7}$$

The resolution is 50×50 gridpoints. Since $x < 0$, the temperature xW_{zz} increases to the northwest in the case of (5.5b), and to the southwest in the case of (5.6b).

Figure 6 shows that the solution with boundary conditions (5.5) closely resembles the outer solution (3.19), with a front (Fig. 6b) at the depth predicted by (3.20). As expected from the theory, the thickness of this front increases with μ. In contrast, the solution with boundary conditions (5.6) does not show a front (Fig. 7b), and the whole solution changes very little if μ is increased by a factor of 5. (The small wiggles in Figure 7, which are caused by a slightly under-resolved diffusive boundary layer at $y = 0$, disappear when μ is increased.) In both experiments, both components u and v of horizontal velocity are negative throughout the fluid (assuming $x < 0$), and have comparable magnitudes. In experiment (5.5) the southwestward horizontal velocity is

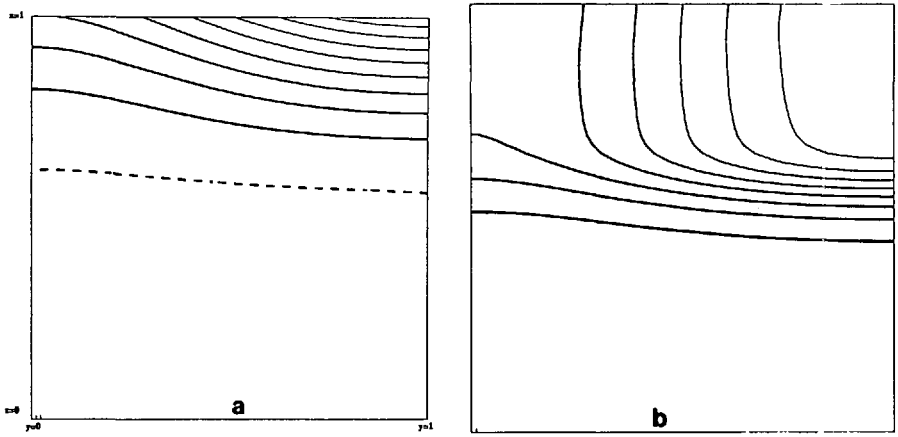

Figure 6. The equilibrium solution to the two-dimensional thermocline model (5.2) with boundary conditions (5.5). This solution agrees closely with (3.19–20). (a) The vertical velocity $W(y, z)$ in a north-south section; and (b) $W_{zz}(y, z)$, which is proportional to the temperature. Darker contours correspond to higher values. The zero contour is dashed.

exactly tangent to surfaces of constant temperature and thus causes no advection of temperature. In experiment (5.6) the southwestward horizontal velocity crosses isotherms, and the steady state is a balance between horizontal and vertical advection.

At this point, there is no reason to assume that the experiment (5.5) with the front is more typical of the ocean than (5.6); indeed, the relationship (5.4) between surface temperature and vertical velocity seems quite special. However, the existence of a thermocline in the real ocean, and the connection established here between the cancellation of the horizontal advection terms and the existence of a front, together

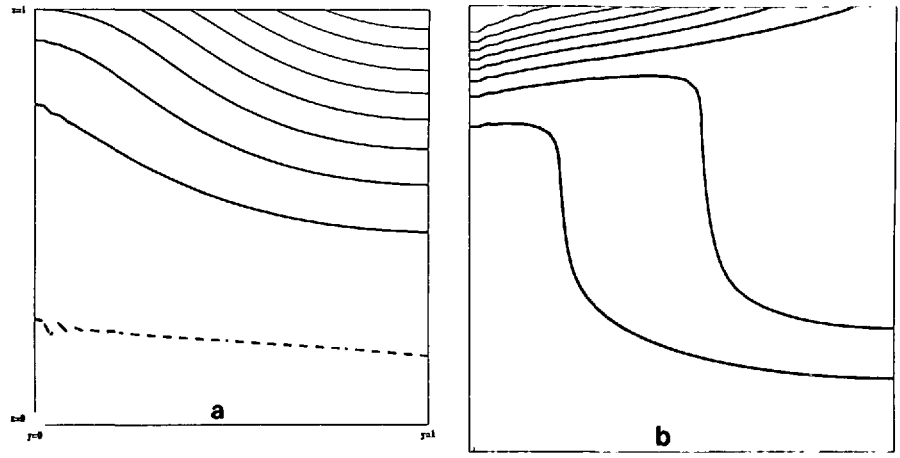

Figure 7. The same as Figure 6, but with the boundary condition (5.6), for which the horizontal advection of temperature is significant. This solution contains no front.

Table 1. Summary of three-dimensional experiments.

Experiment	Q^*	θ^*	θ_{sfc}	θ_{max}	U_{rms}
$\kappa = .1$	10.	10.	8.35	10.7	1.60
$\kappa = .03$	3.	10.	9.28	10.8	1.75
$\kappa = .01$	1.	10.	9.42	10.7	1.91

suggest that, in the more realistic three-dimensional case where the surface temperature is not prescribed in the limit of small diffusivity, the fluid may spontaneously adjust its surface temperature to produce states like that of Figure 6. We test this hypothesis in the following section.

6. Three-dimensional model

In this section, we examine numerical solutions of the fully three-dimensional inertia-less equations (2.5), including viscosity, but still excluding the Ekman layer at the surface. That is, we solve (2.5) with $\mathbf{u}_E = 0$ and surface boundary condition

$$w(x, y, 1) = w_E(x, y). \tag{6.1}$$

The velocity boundary condition at all other boundaries is no-normal-flow. The boundary conditions on the temperature are

$$\theta(x, y, 0) = 0 \tag{6.2}$$

at the bottom, and no-flux at all other boundaries. Temperature contrast is maintained by a heating term $Q(x, y, z)$ added to the right side of (2.5d). This heating term is positive near $z = 1$ and zero elsewhere. In the limit of small temperature diffusivity, a very weak Q can maintain a realistic temperature contrast. In this limit, the temperature throughout the fluid is nonlocally determined by advection. The boundary condition (6.2) and the restriction to positive Q maintain static stability.

In regions where the viscosity is negligible, the solutions to (2.5) also satisfy the thermocline equations in the form (2.21). Suppose that the horizontal advection terms in (2.21) cancel. Then, in the region where two layers are present, the outer solutions

$$M = \frac{1}{2}\theta_E(x, y)(z - 1)^2 + C(x, y)(z - 1) + \frac{f^2}{\beta}\int_{x_0(y)}^{x} w_E(x', y)\, dx', \qquad z > z_0(x, y) \tag{6.3}$$

and

$$M = D(x, y)z + E(y), \qquad z < z_0 \tag{6.4}$$

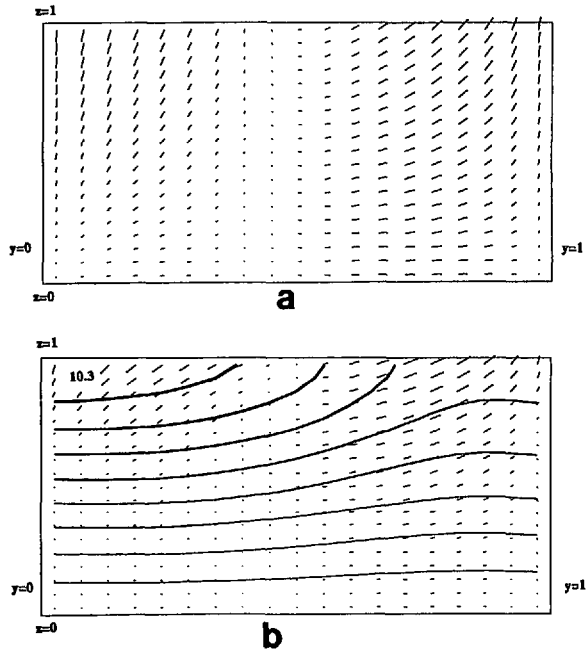

Figure 8. The velocity (arrows) and temperature in a north-south section at mid-basin ($x = 1/2$) with Ekman velocity (6.18) in the case of (a) homogeneous fluid; and for the stratified experiments summarized in Table 1: (b) experiment $\kappa = .1$; (c) experiment $\kappa = .03$; and (d) experiment $\kappa = .01$. The vertical velocity varies between ± 1 at the surface, and the northward velocity has a comparable magnitude (as shown). The maximum temperature in each section is given. The temperature at the bottom, $z = 0$, is constrained to be zero. Darker contours correspond to higher values of the temperature.

satisfy the boundary conditions on vertical velocity and temperature, and the thermocline equations (2.21) *provided that*

$$J(C, \theta_E) \equiv \frac{\partial(C, \theta_E)}{\partial(x, y)} = 0. \tag{6.5}$$

Equation (6.5) is the requirement that the horizontal advection terms cancel. The functions

$$\theta_E(x, y), \qquad C(x, y), \qquad x_0(y), \qquad D(x, y), \qquad E(y), \qquad z_0(x, y) \tag{6.6}$$

must be determined from boundary and matching conditions. The jump conditions at the front $z = z_0(x, y)$ can be succinctly written as

$$\Delta M = 0 \tag{6.7}$$

$$\Delta(M_z) = 0 \tag{6.8}$$

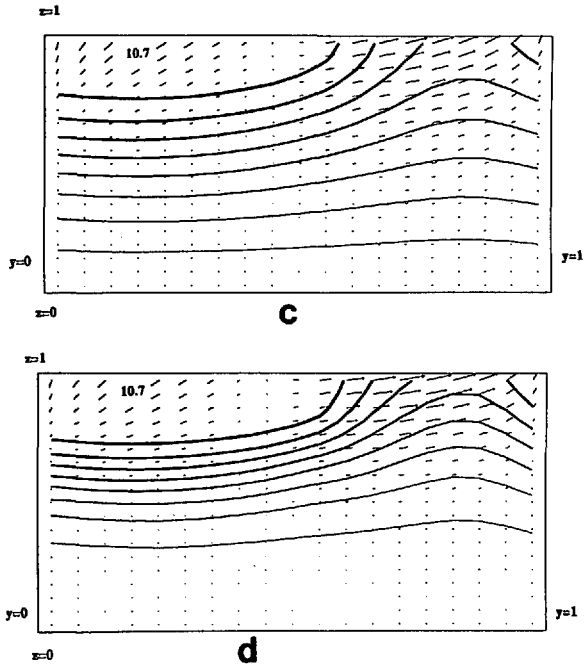

and

$$w = \mathbf{u} \cdot \nabla z_0 \qquad \text{at} \qquad z = z_0^+ \qquad \text{and} \qquad z = z_0^-. \tag{6.9}$$

Eqs. (6.7) and (6.8) also imply that $\Delta(M_x) = \Delta(M_y) = 0$, so that

$$\Delta w = 0. \tag{6.10}$$

Further, (6.8) implies that

$$f\Delta v = -\Delta\theta \frac{\partial z_0}{\partial x} \qquad \text{and} \qquad f\Delta u = \Delta\theta \frac{\partial z_0}{\partial y} \tag{6.11}$$

which are the thermal wind equations integrated across the front. Then by (6.10) and (6.11), the jump in equation (6.9) across the front is zero. Thus the only independent jump conditions are (6.7), (6.8) and (6.9) in (say) the bottom layer. Applying these three conditions to (6.3–4) we obtain

$$C = \theta_E h + D, \tag{6.12}$$

the integrated Sverdrup relation,

$$\frac{1}{2}\theta_E h^2 = \frac{f^2}{\beta}\int_{x_0}^{x} w_E \, dx' - D - E \tag{6.13}$$

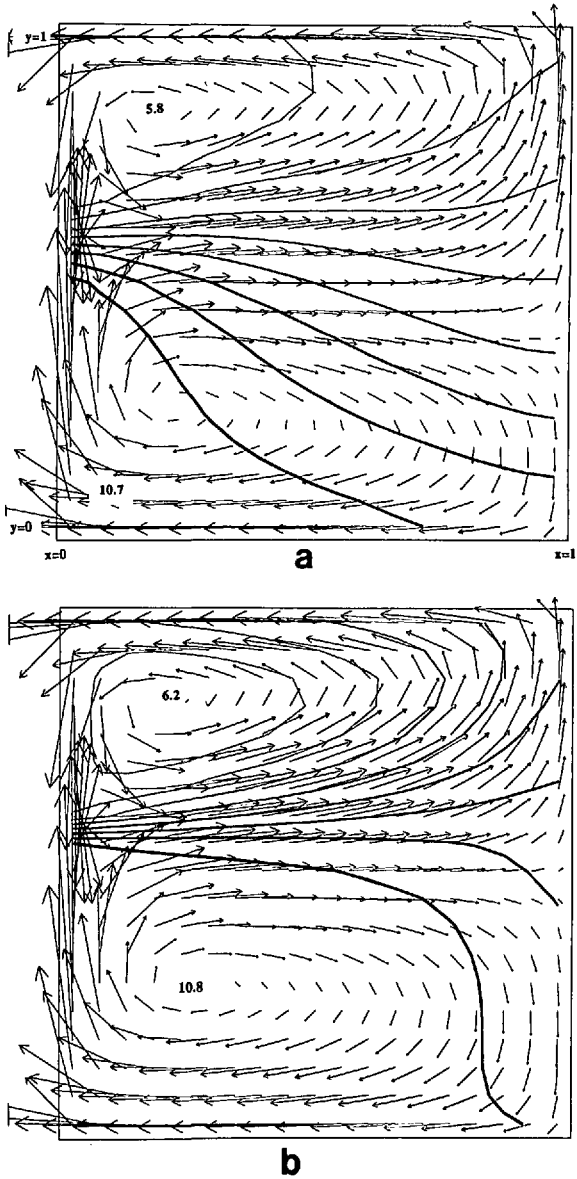

Figure 9. The horizontal velocity and temperature at the surface, $z = 1$, in (a) experiment $\kappa = .1$; (b) experiment $\kappa = .03$; and (c) experiment $\kappa = .01$. The extremal temperatures are given in each picture, and the rms horizontal velocities are 2.4, 2.7 and 3.1 (respectively).

and the potential vorticity equation for the bottom layer,

$$J(D, f/z_0) = 0. \tag{6.14}$$

If the fluid below the front is nearly at rest (as in the numerical experiments of this section) then $D = E = 0$, $C = \theta_E h$, and (6.13) reduces to a generalization of (4.21), viz.

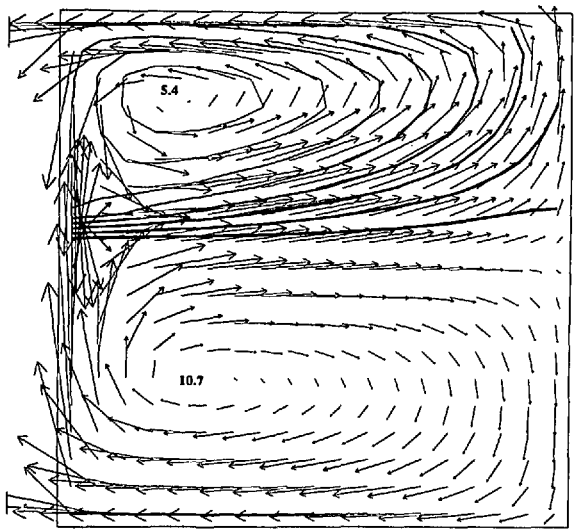

c

$$\frac{1}{2}\theta_E h^2 = \frac{f^2}{\beta}\int_{x_0}^{x} w_E(x', y)\, dx'. \tag{6.15}$$

(Note that w_E differs by a factor of f^2/β from its definition in the previous three sections.) However, (6.5) must still be satisfied. With (6.15), (6.5) becomes

$$J(\theta_E, h) = 0. \tag{6.16}$$

That is, the horizontal advection terms cancel only if the upper-layer temperature is constant along lines of constant thermocline depth.

In this section, we analyze the three numerical experiments summarized in Table 1. These experiments differ mainly in their values for the diffusivity $\kappa = \kappa_h = \kappa_v$. In all three experiments, the prescribed Ekman velocity is

$$w_E(x, y) = -\cos \pi y, \qquad 0 < y < 1 \tag{6.17}$$

corresponding to a southern subtropical wind gyre on $y < 1/2$, and a subpolar gyre on $y > 1/2$. The temperature contrast is maintained by a heating

$$Q(y, z) = \begin{cases} Q^* \cdot (1 - 2y)e^{-(1-z)/\Delta z}(\theta^* - \theta_{sfc}), & y < 1/2 \\ 0, & y > 1/2 \end{cases} \tag{6.18}$$

added to the right-hand side of (2.5d). Here, Q^* and θ^* are prescribed constants, Δz is the vertical grid spacing, and θ_{sfc} is the average surface temperature. Note that Q is nonzero only in the subtropical gyre and near the surface, and "turns off" as the average surface temperature approaches θ^*.

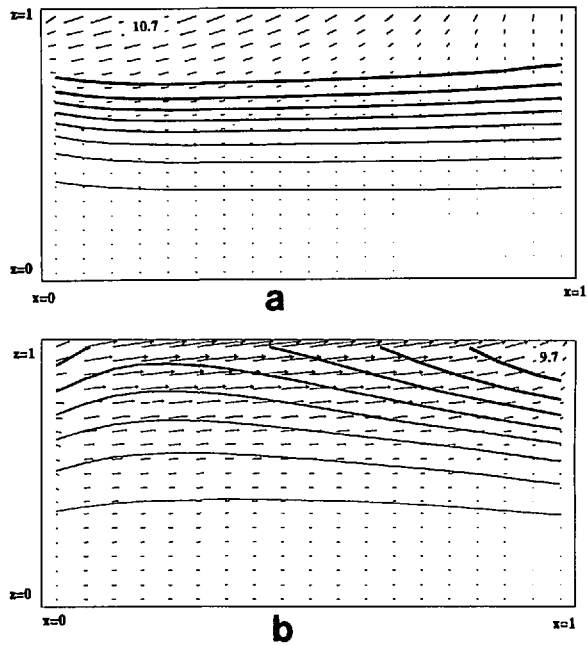

Figure 10. The velocity and temperature in the experiment $\kappa = .01$ at two latitudinal sections, (a) through the subtropical gyre at $y = 1/4$; and (b) through the subpolar gyre at $y = 3/4$. The maximum temperatures are given.

The numerical experiments have a resolution of 20 × 20 × 20 grids, and use the finite-difference advection/diffusion scheme developed by Fiadeiro and Veronis (1977). (All previous experiments used ordinary centered differencing.) In the limit of small diffusivity (at fixed resolution), the Fiadeiro-Veronis scheme shifts from centered differencing of the temperature advection terms to upwind differencing. Therefore, the Fiadeiro-Veronis scheme corresponds, in essence, to an effective local diffusivity in the i-th direction that is the *larger* of $v_i \Delta_i$ and κ, where v_i is the velocity in the i-th direction and Δ_i is the grid spacing. This diffusivity is near the minimum that the spatial resolution will permit.

The Fiadeiro-Veronis scheme is necessary in the three-dimensional experiments because the affordable resolution is not great. In the experiments reported here, centered differencing becomes unstable at diffusivities between $\kappa = .1$ and .03, where the temperature field develops unresolvable small scales. The experiment $\kappa = .1$ was insensitive to the choice between centered differencing and Fiadeiro-Veronis. The experiments $\kappa = .03$ and $\kappa = .01$ could be performed only with Fiadeiro-Veronis. In these latter two experiments, the effective numerical diffusivity is larger than $\kappa = .03$ and .01 in regions of high velocity. However, useful inferences can still be drawn. Moreover, since the computer time needed to reach equilibrium increases as the fourth power of the grid-spacing, this situation must be allowed to stand.

Once again, all the experiments converge toward a steady state. Table 1 gives the average surface temperature, the maximum temperature θ_{max}, and the rms horizontal velocity U_{rms} at the end of each experiment (after 3000 timesteps). Figure 8 shows the velocity and temperature in a north-south section at $x = \frac{1}{2}$. As the temperature diffusivity decreases, the front corresponding to the thermocline sharpens, and the subtropical wind-driven flow is confined to the layer above the thermocline. In the subpolar gyre, the wind-driven flow penetrates more deeply. In homogeneous fluid (Fig. 8a), the horizontal flow would be depth-invariant.

Figure 9 shows the velocity and temperature at the surface, $z = 1$. As the diffusivity decreases, the surface temperature resembles the heating (6.18) less and less, and the horizontal velocity aligns itself with the isotherms.

In the limit $\kappa \to 0$, our theory predicts that the flux of both mass and heat across the thermocline front must be zero. This follows from the facts that the velocity normal to the front is asymptotically zero, and the diffusive temperature flux across the front decreases as $\kappa^{1/2}$. Therefore, the imposed Ekman mass flux into the subtropical upper layer must escape at the boundary $y = \frac{1}{2}$ between gyres, where the front breaks down. In the subpolar gyre, a front cannot exist because of Ekman *upwelling*.

Figures 9c and 10 show that the sharp front does indeed disappear as warm fluid crosses the boundary between gyres. The temperature variance created by Q in the subtropical gyre disappears as the warm fluid, circulating in the subpolar gyre, flows back into the Ekman layer.

Figure 11 shows the thermocline depth (defined somewhat arbitrarily as the depth of maximum vertical temperature change) and the surface temperature in the subtropical gyre, $y < \frac{1}{2}$. A visual comparison between the top and bottom pictures in Figure 11 tests the relationship (6.16) needed to satisfy the hypothesis that the horizontal advection of temperature is negligible. As the diffusivity decreases (from Figure 11a to 11c) the isolines of thermocline depth and surface temperature tend to coincide.

This conclusion is reinforced by Figure 12, which offers a more direct test of the alignment between the horizontal velocity and the isotherms. Figure 12 shows that the angle between the horizontal velocity and the isotherms on level surfaces tends to zero as $\kappa \to 0$. (The relatively large angles at small z are somewhat irrelevant, because the deep velocity is very small.)

Finally, we note from Figures 9 and 11 (top) that, as κ decreases, the temperature contrast *within* the subtropical upper layer decreases dramatically. Again, this occurs because the heat flux across the front tends to zero. Heat transfer then occurs only at the boundary between gyres, and the significant proportion of subtropical water that recirculates above the thermocline homogenizes its temperature.

7. Discussion

In my opinion, the most successful inertia-less model of the general circulation is the two-layer model developed by Parsons (1969), Veronis (1973, 1976, 1978, 1981),

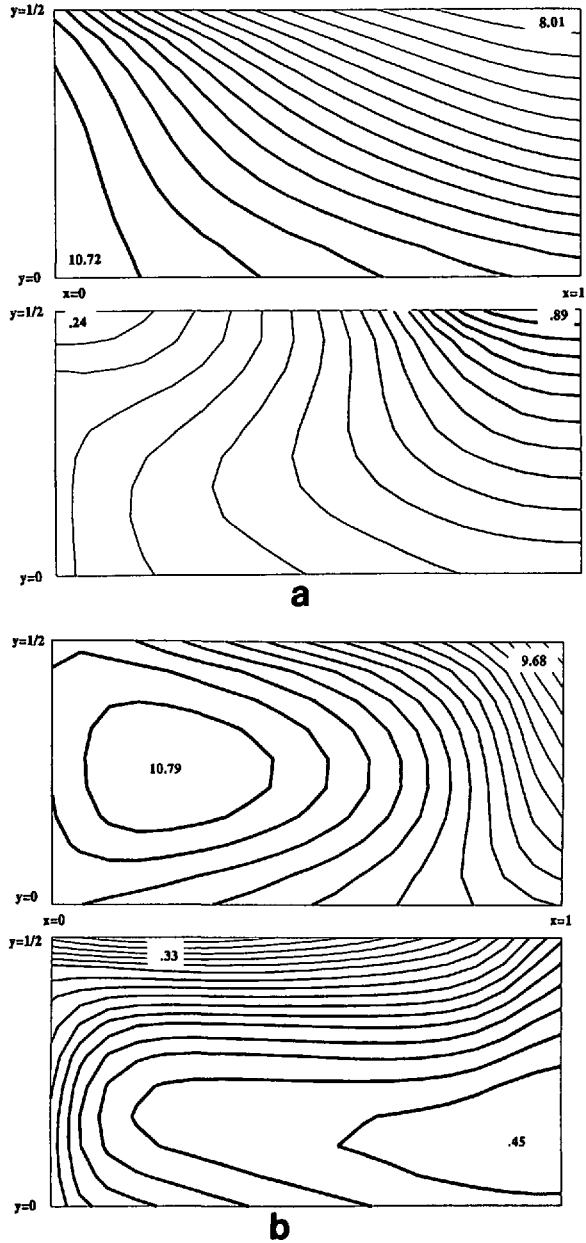

Figure 11. The thermocline depth (bottom) and surface temperature (top) in the subtropical gyre, $0 < y < 1/2$, in (a) experiment $\kappa = .1$; (b) experiment $\kappa = .03$; and (c) experiment $\kappa = .01$. Extremal values are given. Darker contours correspond to higher values.

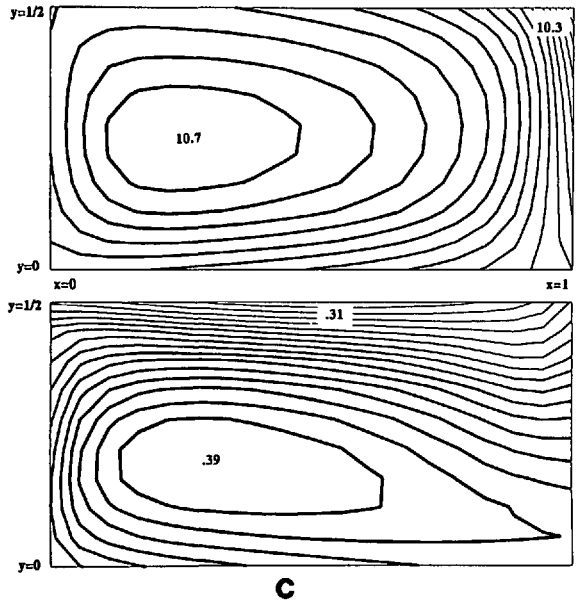

c

Kamenkovich and Reznik (1972), and Huang and Flierl (1987). This model explains many features of the observed circulation on the basis of relatively few special assumptions. However, it does rely on the *assumption* of two density layers separated by a sharp front. The justification for this assumption may be the most important result of the present paper. However, our experiments suggest that the front disappears (except perhaps as a boundary layer at the top) in the subpolar gyre, where the warm water is returned to the bottom layer.

Our results suggest that it is impossible to explain the thermocline structure within the subtropical gyre on the basis of ideal thermocline theory (i.e., without invoking temperature diffusion) as attempted, for example, by Huang (1988). Our picture also differs significantly from that of Luyten, Pedlosky and Stommel (1983), who assume that, in the limit of zero temperature diffusion, the ocean consists of multiple "layers" isolated from surface influence except in narrow outcropping bands. Here we have argued that, in the asymptotic limit, there are only *two* layers, and the upper layer satisfies the boundary conditions at the surface. However, these boundary conditions do not include a *prescribed* temperature at the ocean surface. In contrast to Luyten *et al.*, I believe that it is inconsistent to prescribe the surface temperature in the limit of zero temperature diffusivity.

In our view, the difference between the two-layer state and the observed ocean is caused by a finite temperature diffusivity, which, as we know from the relatively large observed thermocline thickness, is not vanishingly small. This raises the issue of whether the asymptotic case of zero diffusion is even worth considering. I believe that a correct asymptotic theory offers the best hope of physical understanding. Moreover, if

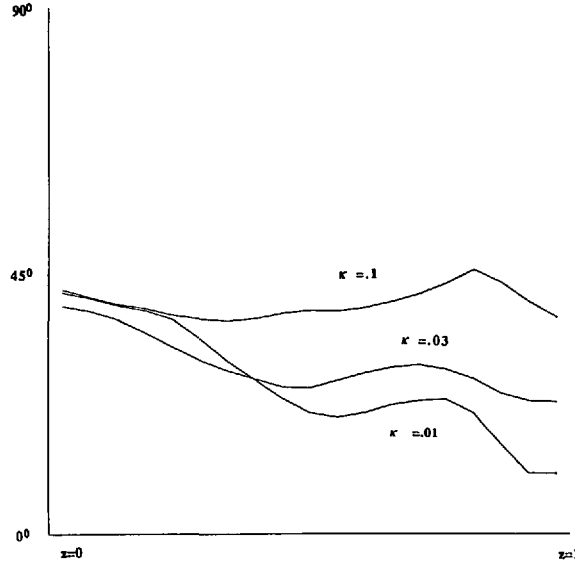

Figure 12. The average angle between the horizontal velocity and isotherms on level surfaces in the three experiments.

the ideas advanced here should hold up, then a next-order theory might provide the needed quantitative accuracy.

We leave completely open the issue of *why* the ocean should choose to arrange itself so that the vertical and horizontal advection of temperature are separately zero. I believe that a fundamental explanation for this is somehow related to the preference of the system for steady state solutions.

Is inertia really negligible in large-scale ocean circulation? Salmon (1982) suggested that the *shape* of the thermocline front is controlled by inertial boundary layers that drive the system toward a statistical-mechanical equilibrium state resembling that discussed by Fofonoff (1954). This suggestion has received some support from the numerical experiments of Griffa and Salmon (1989) with a quasigeostrophic model. However, these experiments also show that the time required to reach statistical equilibrium is very long for a realistically small Rossby number. In the experiments of Griffa and Salmon, the Rossby number was kept large in order to resolve the inertial boundary layers. The question of whether the whole ocean exhibits a significant inertial recirculation is perhaps best answered from observations.

Acknowledgments. This work was supported by the National Science Foundation grants OCE-86-01399 and OCE-89-01720. Numerical experiments were performed on the Cray XMP at the San Diego Supercomputer Center. The San Diego Supercomputer Center is supported by the National Science Foundation. I gratefully acknowledge stimulating discussions with G. R. Ierley and W. R. Young.

REFERENCES

Colin de Verdiere, A. 1988. Buoyancy driven planetary flows. J. Mar. Res., *46,* 215–265.

——1989. On the interaction of wind and buoyancy driven gyres. J. Mar. Res., *47,* 595–633.

Fiadeiro, M. E. and G. Veronis. 1977. On weighted-mean schemes for the finite-difference approximation to the advection-diffusion equation. Tellus, *29,* 512–522.

Fofonoff, N. P. 1954. Steady flow in a frictionless horizontal ocean. J. Mar. Res., *13,* 254–262.

Griffa, A. and R. Salmon. 1989. Wind-driven ocean circulation and equilibrium statistical mechanics. J. Mar. Res., *47,* 457–492.

Huang, R. X. 1988. On boundary value problems of the ideal-fluid thermocline. J. Phys. Oceanogr., *18,* 619–641.

——1989. The generalized eastern boundary conditions and the three-dimensional structure of the ideal fluid thermocline. J. Geophys. Res., *94,* (C4), 4855–4865.

Huang, R. X. and G. R. Flierl. 1987. Two-layer models for the thermocline and current structure in subtropical/subpolar gyres. J. Phys. Oceanogr., *17,* 872–884.

Janowitz, G. S. 1986. A surface density and wind-driven model of the thermocline. J. Geophys. Res., *91,* (C4), 5111–5118.

Kamenkovich, V. M. and G. M. Reznik. 1972. A contribution to the theory of stationary wind-driven currents in a two-layer liquid. Izv. Atmos. Ocean. Phys., *8,* 419–434. (English transl. Atmos. Oc. Phys., *8,* 238–245.)

Luyten, J. R., J. Pedlosky and H. Stommel. 1983. The ventilated thermocline. J. Phys. Oceanogr., *13,* 292–309.

Parsons, A. T. 1969. Two layer model of Gulf Stream separation. J. Fluid Mech., *39,* 511–528.

Pedlosky, J. 1983. Eastern boundary ventilation and the structure of the thermocline. J. Phys. Oceanogr., *13,* 2038–2044.

Robinson, A. and H. Stommel. 1959. The oceanic thermocline and the associated thermohaline circulation. Tellus, *11,* 295–308.

Salmon, R. 1982. The shape of the main thermocline. J. Phys. Oceanogr., *12,* 1458–1479.

——1986. A simplified linear ocean circulation theory. J. Mar. Res., *44,* 695–711.

Stommel, H. and J. Webster. 1962. Some properties of thermocline equations in a subtropical gyre. J. Mar. Res., *20,* 42–56.

Veronis, G. 1973. Model of world ocean circulation: I. Wind-driven, two-layer. J. Mar. Res., *31,* 228–288.

——1976. Model of world ocean circulation: II. Thermally driven, two-layer. J. Mar. Res., *34,* 199–216.

——1978. Model of world ocean circulation: III. Thermally and wind-driven. J. Mar. Res., *36,* 1–44.

——1981. Dynamics of large-scale ocean circulation, *in* Evolution of Physical Oceanography, B. A. Warren and C. Wunsch, eds., MIT Press, 623 pp.

Welander, P. 1971. The thermocline problem. Phil. Trans. Roy. Soc. London, *A270,* 415–442.

Young, W. R. and G. R. Ierley. 1986. Eastern boundary conditions and weak solutions of the ideal thermocline equations. J. Phys. Oceanogr., *16,* 1884–1900.

Received: *27 November 1989;* revised: *14 May 1990.*